Dalton Transactions

PAPER

View Article Online
View Journal | View Issue

CrossMark click for updates

Cite this: *Dalton Trans.*, 2015, **44**, 16119

Nanostructured cobalt hydroxide thin films as high performance pseudocapacitor electrodes by graphene oxide wrapping†

Sangmi Bae,[a] Ji-Hyun Cha,[a] Jong Hyeon Lee[b] and Duk-Young Jung*[a]

Received 8th June 2015,
Accepted 5th August 2015

DOI: 10.1039/c5dt02161h

www.rsc.org/dalton

We synthesized binder-free $Co(OH)_2$ nanocrystals on nickel electrodes by the ammonia transfer method in an aqueous solution and kinetically-controlled their thickness and height to enhance the capacitance through the facile diffusion of electrolytes in the nanocrystals. As thinner $Co(OH)_2$ films were developed, the specific capacitance increased up to 1260 F g^{-1} at a current density of 10 A g^{-1}. A thin layer of graphene oxide (GO) was used to wrap the $Co(OH)_2$ nanocrystals to create a pseudocapacitor with high specific capacitance and good cyclic stability. This synthetic strategy enabled us to maximize the electrochemical cell performance, reaching a specific capacitance of 2710 F g^{-1} under 10 A g^{-1}. The GO coating provides an effective method to increase adhesion on the nickel electrodes and to reduce the decomposition of $Co(OH)_2$ during the charge–discharge process under high pH conditions. The prepared GO/$Co(OH)_2$ nanocomposite layers provided not only high electron mobility but also ionic conductivity, especially when operated at a high current density.

Introduction

Recently, electrochemical supercapacitors (ES) have received attention as a promising next-generation energy storage system because they show higher power densities and larger cycle stability than secondary batteries and show higher energy storage than dielectric capacitors.[1] However, the low energy density and the high production cost of ES materials hinder their practical application. Some representative oxide ES materials that utilize faradaic reactions, such as RuO_2, MnO_2, Co_3O_4, and $Co(OH)_2$, have been studied in order to achieve higher energy densities.[2–4] These energy densities show 10 to 100 times larger capacitance values than electrical double-layer supercapacitors (EDLSs), such as carbon and other materials, based on their surface charge accumulation.[5] Among these, cobalt hydroxide ($Co(OH)_2$) is inexpensive, can be easily prepared, involves a layered crystal structure that allows fast guest ion insertion/desertion reactions because of its large interlayer space, and has the capability for ionic conductivity.[5,6] In addition, cobalt hydroxide has a high theoretical capacitance of 3460 F g^{-1} due to the two-step reversible redox reactions of Co(II) ↔ Co(III) ↔ Co(IV), which makes it a possible pseudocapacitor material.[7,8] The main research issue facing $Co(OH)_2$ is how to improve its low cycle stability, small potential window, and power density. Additionally, the development of an optimized ES:EDLS hybrid system, through the syntheses of novel composite materials, is appealing.[9–12] For instance, although the enlarged surface area of nanometer-sized $Co(OH)_2$ particles grown on nickel metal substrates has resulted in an increase in the specific capacitance under low current densities (up to 1782 F g^{-1}), the same sample showed a remarkably small specific capacitance under a high current density (10 A g^{-1}).[3] Conversely, α-$Co(OH)_2$ directly grown on graphite substrates showed higher conductivity and a larger surface area for the active materials, maintaining a high specific capacitance (83% of the low current density value) under high current density conditions (10 A g^{-1}) and excellent stability up to 5000 cycles.[13]

This study presents a methodology to maximize the electrochemical cell performance data (*e.g.*, the specific capacitance, cyclic stability, and specific capacitance) by considering the chemical composition and the nanostructure of the active materials. First, the ammonia transfer syntheses enabled us to prepare $Co(OH)_2$ nanostructure films that are directly deposited on a nickel electrode as a current collector without the need for surfactants and/or binder materials, which can decrease the energy density and capacitance.[14–16] Secondly,

[a]*Department of Chemistry, Center for Human Interface Nanotechnology, SKKU Advanced Institute of Nanotechnology, Institute of Basic Science, Sungkyunkwan University, Suwon 440-746, Republic of Korea. E-mail: dyjung@skku.edu*
[b]*Department of Chemistry, The Catholic University of Korea, Bucheon, 420-743, Republic of Korea*

†Electronic supplementary information (ESI) available: SEM images, sample photographs, Raman mapping, zeta potential, elemental analysis data and electrochemical measurement data of GO, $Co(OH)_2$ and GO wrapped $Co(OH)_2$ samples. See DOI: 10.1039/c5dt02161h

the conformal thin layers of $Co(OH)_2$ deposited on planar substrates generally showed low electrode performance due to the lower electrochemical contribution of the inner layer active material.[16] Conversely, three-dimensional porous electrodes gave higher efficiencies with the same deposited mass due to their higher surface areas.[17] In the present study, we deposited vertically-grown $Co(OH)_2$ nanoplates directly on the form-type nickel metal substrates, which significantly increased the specific area of the three-dimensional nanostructures.[3,7] The specific surface area was increased most significantly when $Co(OH)_2$ nanoplates (as thin as 20 nm) were obtained by the kinetic control method (without an etching process). The increase in the specific area can reduce the ion diffusion path, which results in an increase in the ionic and electronic conductivities.[3,16] Thirdly, we wrapped a thin layer of graphene oxide (GO) around the $Co(OH)_2$ nanoplates on the nickel electrodes. This provided various benefits, including increasing the adhesion on the nickel electrodes and reducing the dissolution/decomposition of $Co(OH)_2$ during the charge–discharge process under high pH conditions.[18] The prepared GO/$Co(OH)_2$ nanocomposite layers provided not only high electron mobility[19] but also ionic conductivity,[20] especially when operated at a high current density. So far, graphite and graphene have been used as surface modifiers on metal electrodes to improve the conductivity.[21]

Results and discussion

Morphology of cobalt hydroxides and graphene oxide wrapped cobalt hydroxides

Fig. 1 demonstrates the synthetic method used to produce GO/$Co(OH)_2$/nickel form hybrid electrodes. The monodispersed, green-colored nanoplates of α-$Co(OH)_2$ layered hydroxide salts were deposited on the form-type nickel substrates by the ammonia gas transfer method. The vertical lengths and thicknesses of α-$Co(OH)_2$ nanoplates increased with the reaction time: the vertical length was 3 μm after 12 h and 10 μm after 24 h (Fig. S1 and S2†).

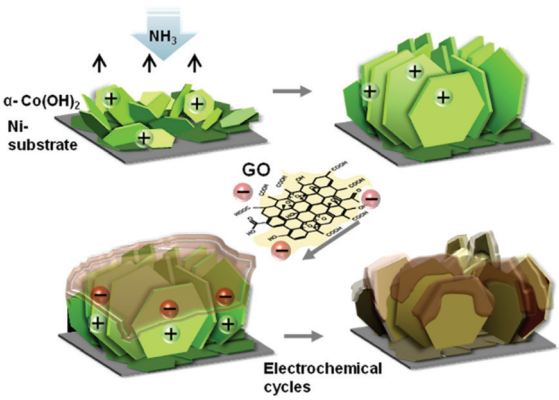

Fig. 1 Schematic description of the synthesis process of GO-wrapped $Co(OH)_2$.

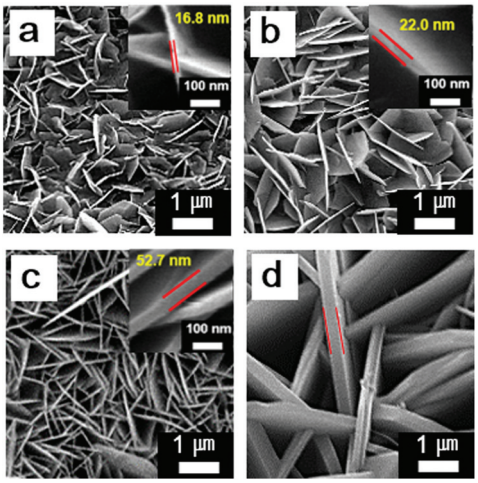

Fig. 2 SEM images of $Co(OH)_2$ with reaction times of (a) 20 min, (b) 40 min (two 20 min reactions), (c) 6 h, and (d) 18 h.

The morphology and thickness of the deposited $Co(OH)_2$ nanoplates were observed by SEM, as shown in Fig. 2. After a reaction time of 20 min, the $Co(OH)_2$ nanoplates (Fig. 2a) grew horizontally with a nanoplate thickness of 14 nm and showed partial coverage of the nickel substrates. Repeating two 20 min depositions, denoted as $Co(OH)_2$-40m (Fig. 2b), produced 20 nm-thick $Co(OH)_2$ with full coverage. Deposition times of 6 h (denoted as $Co(OH)_2$-6h) and 18 h (Fig. 2c and d) produced vertically-grown $Co(OH)_2$ nanoplates with 50 nm and 310 nm thicknesses, respectively. Shorter reaction times produced smaller thicknesses, shorter vertical lengths, and lower deposited masses.[22] High surface area and strong adhesion of $Co(OH)_2$ on the nickel substrates are important factors for pseudocapacitor application. We compared the electrochemical properties of the $Co(OH)_2$-40m samples with the $Co(OH)_2$-6h samples.

Fig. 3 describes the detailed wrapping mechanism of the GO nanosheets on the $Co(OH)_2$-6h samples. The GO nanosheets were fully adsorbed on the hexagonal nanoplates of $Co(OH)_2$ *via* the electrostatic attraction between the positive $Co(OH)_2$ and the negative GO surface zeta potentials. The layer-by-layer coating was achieved by mixing two colloidal solutions of $Co(OH)_2$ and GO, which produced instant aggregation, demonstrating their strong interaction (Fig. S3 and S4†). The GO wrapping on $Co(OH)_2$ can also be confirmed by the color change from green to light brown (Fig. S5†). The electron micrograph indicated that the $Co(OH)_2$ nanoplates under the GO layers remained perpendicularly-oriented to the nickel substrate surface after the GO wrapping (Fig. 3b, f and j). The irregular size distribution and dense vertical packing of $Co(OH)_2$ nanoplates were incorporated with the free-standing GO nanosheets like a blanket on trees.

The effects of the GO coating on the electrochemical charge–discharge experiments were surprising. 1000 charge–discharge cycles for $Co(OH)_2$ without the GO layers completely destroyed the hexagonal shapes of the $Co(OH)_2$ nanoplates,

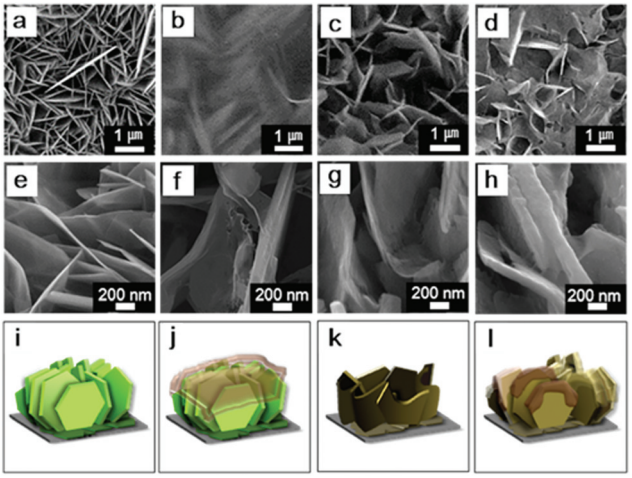

Fig. 3 (a, e, i) SEM images and schematic illustrations of $Co(OH)_2$-6h, (b, f, j) GO-wrapped $Co(OH)_2$-6h, (c, g, k) $Co(OH)_2$-6h after 1000 cycles, and (d, h, l) GO-wrapped $Co(OH)_2$-6h after 1000 cycles.

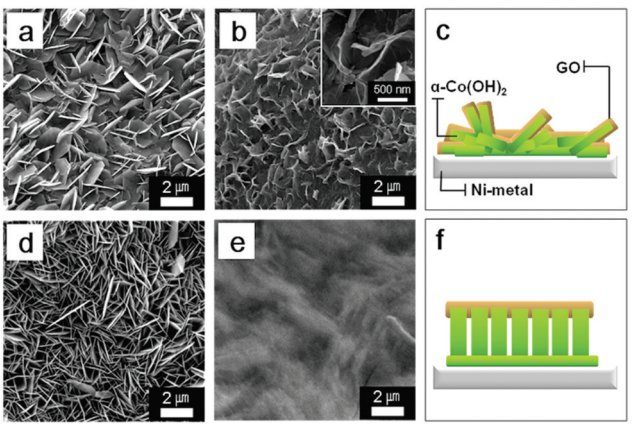

Fig. 4 SEM images and schematic illustrations of (a) $Co(OH)_2$-40m, (b, c) GO-$Co(OH)_2$-40m, (d) $Co(OH)_2$-6h, and (e, f) GO-$Co(OH)_2$-6h.

severely bending and distorting their edges (Fig. 3c, g and k).

Conversely, the $Co(OH)_2$ with GO layers held their hexagonal shapes and demonstrated tighter contact between the $Co(OH)_2$ and GO after the same charge–discharge experiments (Fig. 3d, h and l). Although $Co(OH)_2$ samples with GO and without GO both showed a dark brown color, the $Co(OH)_2$ wrapped by GO presented pristine hexagonal shapes, indicating that both an improved structural stability and superior electrochemical characteristics were provided by the presence of the GO layers (*vide infra*). The coverage patterns of the GO on $Co(OH)_2$ depended upon the conformation of the $Co(OH)_2$ nanoplates, as shown in Fig. 4. For example, $Co(OH)_2$-40m (grown in a short reaction time) demonstrated a small tilting angle with the nickel surface and a curved conformal GO coating along the $Co(OH)_2$ surface. Alternatively, the GO layer of $Co(OH)_2$-6h, with the vertically preferred orientation, formed a flat GO surface at the top edges of the $Co(OH)_2$ nanoplates rather than the face-to-face coating that was observed in $Co(OH)_2$-40m. We expect that, compared to $Co(OH)_2$-6h, $Co(OH)_2$-40m has a larger direct contact area between the $Co(OH)_2$ and GO and a smaller void space, both of which can influence the electrochemical properties.

Electrochemical properties of cobalt hydroxides

The electrochemical properties of $Co(OH)_2$-6h and $Co(OH)_2$-40m were measured in a 2 M KOH solution using a three electrode system. The cyclic voltammetry (CV) data were collected between −0.2 and 0.5 V at a scan rate ranging from 5 to 100 mV s^{-1}. The CV curve for $Co(OH)_2$-6h (Fig. 5-1a) showed two redox peaks: one from 0.030 to 0.113 V and another from −0.035 to −0.107 V. These were assigned to the quasi-reversible reaction from $Co(OH)_2$ to CoOOH (eqn (1)).[2,9,17,23,24] The cyclic voltammetry analyses have been performed in the range of −0.2 to 0.5 V as a full window of potentials in order to investigate the significant irreversible oxidation peak near 0.4 V, as shown in Fig. S6, S7 and S9.† However, we carried out the charge–discharge cycles in the narrower potential range of 0.1–0.4 V, where the electrochemical reaction occurs in the regime of quasi-reversible oxidation–reduction for all the samples. Based on the position of the secondary oxidation peak (O2) near 0.3 V in CV curves of Fig. 5(1a and 2a) and Fig. 6(1a and 2a), we chose 0.4 V as a maximal positive potential in all galvanostatic discharge measurements.

$$Co(OH)_2 + OH^- \leftrightarrow CoOOH + H_2O + e^- \quad (1)$$

As the scan rate increases, the anodic peak shifted to a positive potential, while the cathodic peaks moved in the negative direction. This increased difference between the two redox peaks is attributed to the electrode resistance and polarization resulting from the slow faradaic process.[25,26] The GO-wrapped $Co(OH)_2$-6h (denoted as GO-$Co(OH)_2$-6h) showed oxidation between −0.010 and 0.062 V and reduction between −0.047 and −0.102 V (Fig. 5-2a). The GO-$Co(OH)_2$-6h presented a similar CV curve shape to $Co(OH)_2$-6h. However, a larger area of the CV curve and a smaller potential difference between the oxidation and reduction, as compared to the $Co(OH)_2$-6h, were observed due to the shift to smaller values of the oxidation peaks. The effect of GO wrapping was also observed in GO-$Co(OH)_2$-40m (Fig. S6†), indicating the prominent contribution of GO to the increased electrochemical reaction kinetics.[27] The redox potentials after 1000 cycles were changed significantly due to the oxidation reaction of $Co(OH)_2$ in a basic solution (Fig. S7†), as shown in eqn (2):[23]

$$Co_3O_4 + 4OH^- \leftrightarrow 3CoO_2 + 2H_2O + 4e^- \quad (2)$$

The discharge time of the galvanostatic measurement increased in GO-wrapped films for all current density conditions (Fig. 5b). The specific capacitances were estimated according to the following equation (eqn (3)), in the potential range of −0.1 to 0.4 V:

$$C_m = c/m = (I \times \Delta t)/(\Delta V \times m) \quad (3)$$

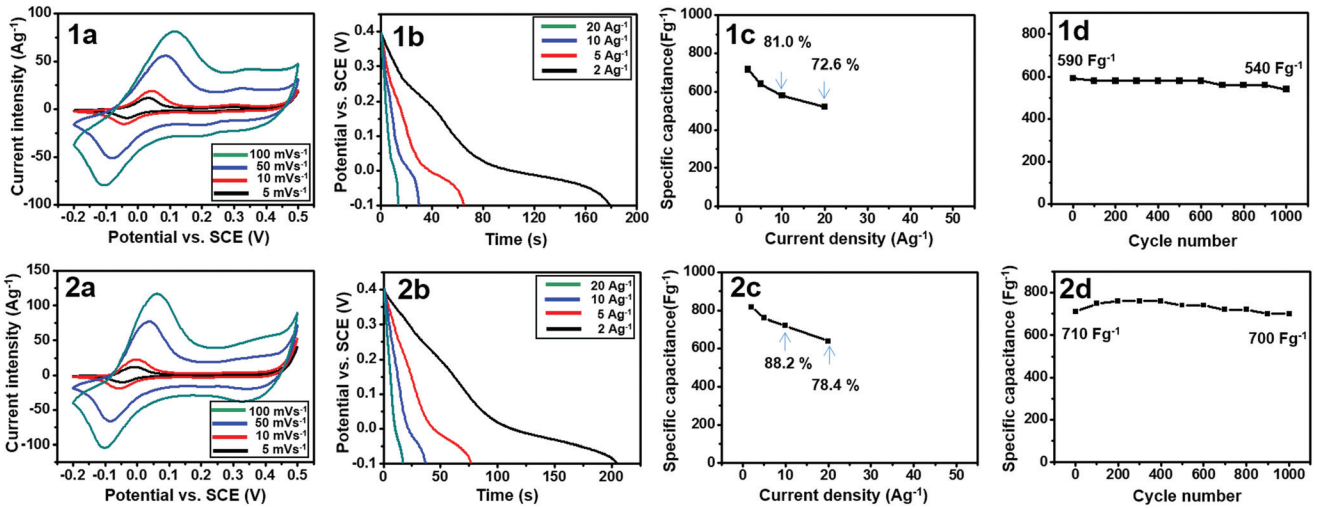

Fig. 5 Electrochemical characterization of (1) $Co(OH)_2$-6h and (2) GO-wrapped $Co(OH)_2$-6h. (a) CV curves, (b) galvanostatic discharge curves, (c) specific capacitance *versus* current density, and (d) plots of specific capacitance *versus* cycle number.

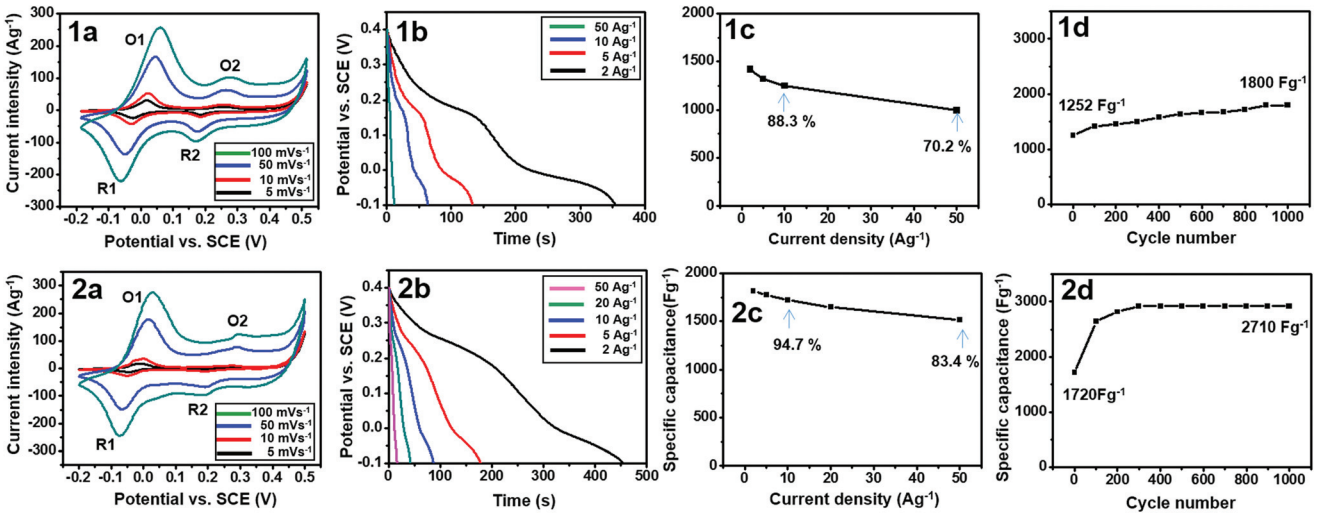

Fig. 6 Electrochemical characterization of (1) $Co(OH)_2$-40m and (2) GO-wrapped $Co(OH)_2$-40m. (a) CV curves, (b) galvanostatic discharge curves, (c) specific capacitance *versus* current density, and (d) plots of specific capacitance *versus* cycle number under 10 A g^{-1}.

where C_m is the specific capacitance, I is the discharge current, t is the charge time, V is the voltage, and m is the mass of $Co(OH)_2$.

The specific capacitances of $Co(OH)_2$-6h decreased from 716 F g^{-1} (2 A g^{-1}) to 520 F g^{-1} (20 A g^{-1}), maintaining 81.0% (10 A g^{-1}) and 72.6% (20 A g^{-1}) of the capacitance measured at 2 A g^{-1} (Fig. 5c). The specific capacitances of GO-$Co(OH)_2$-6h were 816 F g^{-1} (2 A g^{-1}) and 640 F g^{-1} (20 A g^{-1}), demonstrating the large improvement caused by GO wrapping (an increase between 100 and 140 F g^{-1}). We note that the stability of the specific capacitance imparted by GO wrapping was improved up to 88.2% and 78.4% of the capacitances under high current density conditions. The specific capacitance as a function of 1000 charge–discharge cycles was evaluated under 10 A g^{-1}. The $Co(OH)_2$-6h showed a loss of 8.5% of the initial capacitance after 1000 cycles, but the loss of GO-$Co(OH)_2$-6h was only 1.4%. This indicates that the GO wrapping enhances the stability of the current density as well as increasing cyclic stability (Fig. 5d).

The improvement in capacitor performance caused by GO wrapping was even more outstanding in the nanostructured, large surface area sample ($Co(OH)_2$-40m). The CV curves of $Co(OH)_2$-40m and GO-$Co(OH)_2$-40m produced similar shapes. When larger scan rates were applied, higher current densities were obtained (Fig. 6a). The curves possess four peaks: the oxidation-1 (0.018 to −0.061 V) and reduction-1 (−0.027 to −0.062 V) correspond to the redox reaction of cobalt hydroxides (described in eqn (1)), and the oxidation-2 (0.258 to

0.275 V) and reduction-2 (0.187 to 0.172 V) correspond to the redox reaction of the nickel substrates (Fig. 6).[26] The contribution of nickel to the electrochemical measurements was reduced to below 5% due to the repeated deposition of cobalt hydroxide on the nickel substrates (Table S1†). The GO-Co(OH)$_2$-40m showed oxidation-1 (−0.013 to 0.029 V) and reduction-1 (−0.045 to −0.072 V) peaks. These represented the smallest shifts in the redox peaks as a function of scan rate among the four prepared samples, implying the best charge–discharge reversibility.[7] The oxidation-2 and reduction-2 peaks became negligible in GO-Co(OH)$_2$-40m; this was ascribed to the increase in the coverage of the electrode surface that was obtained by GO wrapping.

The specific capacitances of Co(OH)$_2$-40m were 1418 F g^{-1} (2 A g^{-1}) and 995 F g^{-1} (50 A g^{-1}), which were two times larger compared to Co(OH)$_2$-6h. The enhancement of the capacitance in nano-sized layers has been reported to be two times higher in the nano arrays of Co(OH)$_2$ fabricated by chemical etching in a basic solution compared to the pristine films.[3] The current study presents a constructive way to produce nanoplates of Co(OH)$_2$ on nickel substrates without harsh etching conditions, which can decompose the crystal structure and particle morphology. The capacitance of GO-Co(OH)$_2$-40m gave the highest values among the four samples (1816 F g^{-1} at 2 A g^{-1} and 1514 F g^{-1} at 50 A g^{-1}), maintaining very high stability under high current conditions, *e.g.*, 94.7% (10 A g^{-1}) and 83.4% (50 A g^{-1}) of the capacitances, which are 13.2% larger than those of Co(OH)$_2$-40m. The synergetic effect of the large open surface of Co(OH)$_2$ nanoplates and the conformal coverage of the GO layer (as shown in the SEM data) contribute to the excellent capacitance performance of GO-Co(OH)$_2$-40m in high current density.

The monotonous increase of the capacitance of Co(OH)$_2$-40m up to 1000 cycles partly results from the formation of defects by dissolution and the increased surface area through electrochemical reactions, which was supported by the morphological changes from the flat to folded forms for the as-prepared Co(OH)$_2$-40m and the samples after the cyclic voltammetry measurements as shown in Fig. S8.†

The specific capacitance after 1000 cycles of Co(OH)$_2$-40m (under 10 A g^{-1}) changed from 1252 to 1800 F g^{-1}; this change is attributed to the activation processes of intercalation and deintercalation of the electrochemical species.[24,28–30] Variations in the specific capacitance of GO-Co(OH)$_2$-40m unusually increased from 1720 to 2710 F g^{-1} after 400 cycles and remained constant until 1000 cycles, which is in accordance with the increase of the area under the CV curve (Fig. S9†). The steep increase observed before 100 cycles was assigned to the fast activation of the electrochemical reaction in the interface layer close to electrolytes (where there is a short ion transport distance), which originates from the dense wrapping of the GO layers on the Co(OH)$_2$ nanoplates with a large, direct contact. The gradual increase seen in the later cycles corresponds to the slower activation of the inner layers.[29]

The Nyquist plot from the electrochemical impedance spectroscopy (EIS), measured at 0.3 V from 0.01 to 105 Hz, provided detailed mechanisms about the high specific capacity, large rate capability, and excellent stability of the GO-wrapped samples (Fig. 7). In the low frequency region, the slopes of GO-Co(OH)$_2$-6h were more vertical than those of Co(OH)$_2$-6h, both before and after 1000 cycles, which indicates easier electrolytic diffusion and more ideal capacitive behavior during the charge–discharge cycles.[23,27] In the high frequency region, the first intercept with the real axis reveals the equivalent series resistance of the electrode (Fig. S10†).[27] This result indicates that the GO treatment helps to reduce the electron transfer resistance of Co(OH)$_2$, which is in accordance with the fast electrode kinetics observed in the CV measurements (where the oxidation potentials were shifted).[27] The large charge–discharge cycles gave larger intercepts, which resulted from the oxidation of Co(III) to Co(IV), as shown in eqn (2).

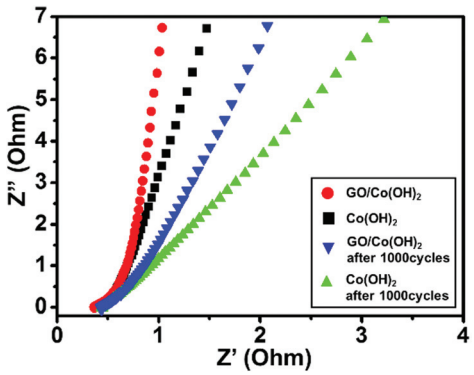

Fig. 7 Nyquist plots of Co(OH)$_2$-6h and GO/Co(OH)$_2$-6h at 0.3 V in the low frequency region.

Analyses of nanostructures by TEM, XRD, and Raman spectroscopy

High-resolution TEM and electron diffraction patterns were used to analyze the crystal structure of Co(OH)$_2$ after GO wrapping (Fig. 8). The lattice image and SAED pattern of Co(OH)$_2$-6h showed the [001] zone axis direction and a clear lattice fringe of 2.69 Å, corresponding to the (100) crystal plane of α-Co(OH)$_2$.[33] The TEM image of GO-Co(OH)$_2$-6h showed a mixture of different phases with good crystallinity. The ED pattern was indexed to cubic Co_3O_4 rather than to Co(OH)$_2$. We outlined two possible explanations for the oxidation of Co(OH)$_2$: either a chemical reaction with the oxygen-bearing functional groups of GO or distortion by electron radiation during the electron microscope measurements.[31] We observed the pattern change of the GO-wrapped Co(OH)$_2$ samples during the ED measurements, taking special interest in the fast change that occurred in the thin Co(OH)$_2$ nanosheets. It should be noted that the Co(OH)$_2$ phase first transforms into the CoOOH structure and then into the Co_3O_4 cubic phase.[32] The absence of any GO spots in the TEM data may be ascribed to the decomposition of the GO layers caused by the presence of accelerated electrons during the TEM measurements.

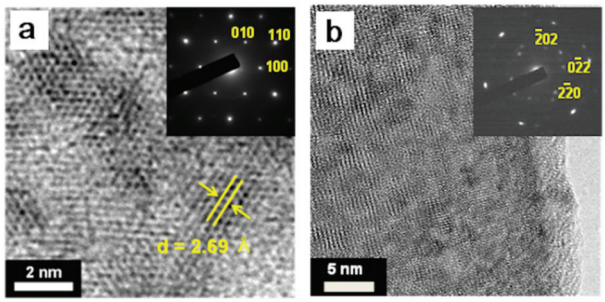

Fig. 8 HRTEM images of (a) $Co(OH)_2$-6h (a) and (b) GO-wrapped $Co(OH)_2$-6h. Inset images are ED patterns.

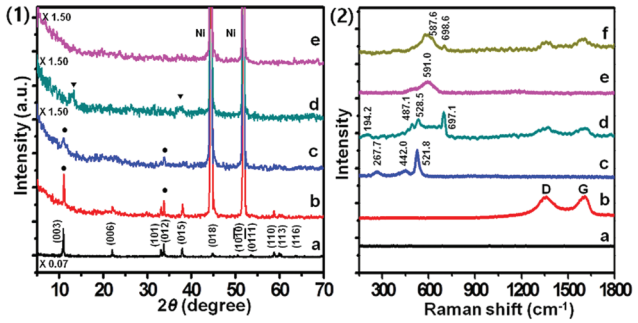

Fig. 9 (1) XRD patterns of (a) $Co(OH)_2$ powder, (b) $Co(OH)_2$ on the Ni-metal substrate ($Co(OH)_2$-6h), (c) GO-$Co(OH)_2$-6h, (d) $Co(OH)_2$-6h after 1000 cycles, and (e) GO-$Co(OH)_2$-6h after 1000 cycles (● = α-$Co(OH)_2$ and ▼ = γ-CoOOH). (2) Raman spectra of (a) the Ni-metal substrate, (b) GO on glass, (c) $Co(OH)_2$-6h, (d) GO-$Co(OH)_2$-6h, (e) $Co(OH)_2$-6h after 1000 cycles, and (f) GO-$Co(OH)_2$-6h after 1000 cycles.

The XRD patterns showed the evolution of the crystal structures in the wrapping and electrochemical reactions (Fig. 9-1). The $Co(OH)_2$ on the nickel form gave peaks that agreed with those observed in bulk samples of the α-$Co(OH)_2$ phase, which has a rhombohedral symmetry ($-h + k + l = 3n$) of a = 3.138 Å and c = 24.06 Å.[22,33] As GO covered the $Co(OH)_2$ nanoplates, the intensity of the XRD peaks decreased (Fig. 9-1c), implying that the adsorption of GO disturbed the surface of $Co(OH)_2$. The internal part of the sample possesses crystallinity, showing the (003) and (012) peaks, which is in agreement with the TEM data in Fig. 8. After 1000 cycles, the XRD pattern of Fig. 9-1d could no longer be matched with α-$Co(OH)_2$ but was indexed as the γ-CoOOH phase.[34,35] This structural transformation was also confirmed by the CV curve after 1000 cycles (Fig. S9†). The XRD peaks of GO-$Co(OH)_2$-6h after 1000 cycles disappeared, yielding an amorphous phase due to its lower crystallinity relative to $Co(OH)_2$-6h. Although the $Co(OH)_2$-40m sample had no apparent peaks in its XRD spectrum (due to the thin layer deposition), HRTEM and SAED revealed crystallinity even after GO wrapping (Fig. S11†).

The $Co(OH)_2$-6h gave the Raman spectra of $Co(OH)_2$ at 267.7 ($E_g(T)$), 447.0 ($A_{1g}(T)$), and 521.8 cm^{-1} ($E_g(R)$).[22] Conversely, GO-$Co(OH)_2$-6h showed the modes of Co_3O_4 at 194.2 (F_{2g}), 487.1 (E_g), 528.5 (F_{2g}), and 697.1 cm^{-1} (A_{1g}),[28,36,37] as well as those of GO at 1357.7 cm^{-1} (D band) and 1605.8 cm^{-1} (G band).[38] The oxidation of the $Co(OH)_2$ surface to Co_3O_4, caused by GO, is in good agreement with the XRD and SAED analyses. The area mapping of the Raman spectra also confirmed the conformal coverage of GO on the $Co(OH)_2$ surface (Fig. S12†). The Raman spectra of both $Co(OH)_2$-6h and GO-$Co(OH)_2$-6h after 1000 cycles showed broad peaks ascribed to various oxidation states of cobalt. The GO peaks remained after 1000 cycles, indicating good adhesion and chemical stability of GO on the cobalt oxide phase.

Conclusions

We successfully synthesized binder-free, surfactant-free GO-$Co(OH)_2$ hybrid electrodes at room temperature under mild conditions and fabricated a pseudocapacitor with high specific capacitance and good cyclic stability. We suggested two factors necessary for obtaining the highest capacitance: an enlarged surface area of thinner nanoplates of $Co(OH)_2$ and GO wrapping of $Co(OH)_2$. As thinner nanoplates were developed, the specific capacitance increased up to 1260 F g^{-1} at a current density of 10 A g^{-1} in the $Co(OH)_2$-40m sample. Additionally, the improvement in the specific capacitance caused by GO wrapping was more significant in the $Co(OH)_2$-40m sample (2710 F g^{-1} under 10 A g^{-1}) than in the $Co(OH)_2$-6h sample, implying that both the conformal coating of the GO layer and a well-developed $Co(OH)_2$ nanostructure are critical to achieve the highest specific capacitance value. The synergetic effects of the high surface area of $Co(OH)_2$ (with a 10 nm-thick nanoplate) and the dense wrapping of the GO layer are under further investigation in an attempt to develop a new GO-$Co(OH)_2$ pseudocapacitor with a high specific capacitance, a high current density, and a high cyclic stability.

Experimental

Synthesis of GO/$Co(OH)_2$/Ni hybrid electrodes

All of the chemical reagents used in this study were purchased from Sigma Aldrich Co. and used as-received without further purification. Nickel foam was purchased from MarkeTech International (≥95% porosity, thickness: 1.6 mm). A nickel foam substrate with a size of 1 cm × 3 cm was cleaned sequentially with acetone and isopropyl alcohol (IPA) with the assistance of ultrasonication for 20 min. The substrate was then dried in an oven at 70 °C. Its top side (1 cm × 1 cm) was protected with polytetrafluoroethylene tape. α-$Co(OH)_2$ nanoplates on the nickel foam were prepared by the ammonia gas diffusion method. All synthesis processes were carried out at room temperature under ambient conditions. A Petri dish and a beaker were placed in a sealed container. The Petri dish was full of an aqueous solution of 0.1 M $CoCl_2 \cdot 6H_2O$ and the beaker was filled with 100 mL of a 0.7% ammonia solution. The prepared nickel foam was hung horizontally on the

surface of the $CoCl_2$ solution and stirred at 150 rpm. Over time, hexagonal α-$Co(OH)_2$ grew perpendicularly from the nickel substrate. After 20 min, α-$Co(OH)_2$ nanosheets on the nickel foam were obtained; these samples were washed with ethanol for 10 min. The experimental formula analyzed by TG, ICP, and EPMA for α-$Co(OH)_2$ is given in Fig. S13 and S14.† In order to obtain denser α-$Co(OH)_2$ films, the deposition process was repeated twice. α-$Co(OH)_2$ on the nickel foam was put into a graphene oxide (GO) solution and stirred weakly for 5 h. GO was prepared by a modified Hummers method.[39] Finally, the GO-wrapped α-$Co(OH)_2$ on the nickel foam was washed with ethanol and dried at 70 °C.

Characterization

The morphologies and the sizes of the obtained products were observed with a Schottky field emission scanning electron microscope (SEM, JSM-7100F) operating at 15 kV. High-resolution transmission electron microscopy (HR-TEM) measurements were carried out using a JEM 2100F. X-ray diffraction (XRD) analyses were performed on a Rigaku Ultima IV diffractometer with Cu Kα radiation ($\lambda \approx 1.54$ Å). Raman spectra were run on a WITec Alpha 300.

Electrochemical measurements

Cyclic voltammetry (CV) and galvanostatic charge–discharge were performed using a PGSTAT302N (Autolab) and electrochemical impedance spectroscopy (EIS) was performed using a potentiostat (VMP3, BioLogic Science Instruments). All electrochemical measurements were carried out in 2 M aqueous KOH in a half-cell setup configuration at room temperature. 2 cm^2 of the α-$Co(OH)_2$ film was used as the working electrode, while a platinum plate electrode and an SCE electrode were used as the counter and reference electrodes, respectively. The mass of the active materials was accurately determined using a microbalance with 10^{-6} g resolution (AnD ION Series Microbalance, BM-22) by calculating the increase in the mass of the nickel foam. EIS measurements were conducted in the frequency range from 0.01 to 100 kHz with an ac perturbation of 0.3 V. The electrochemical signal of the thin layer of GO coating without a $Co(OH)_2$ layer on the Ni electrode was confirmed to be negligible.[40]

Acknowledgements

This work was supported by the Basic Science Research Program (NRF-2009-0094023) and the Center for Human Interface Nano Technology (NRF-2009-0083540).

Notes and references

1 Y. G. Zhu, Y. Wang, Y. Shi, Z. X. Huang, L. Fu and H. Y. Yang, *Adv. Energy Mater.*, 2014, **4**, 1301788.
2 A. D. Jagadale, V. S. Kumbhar, D. S. Dhawale and C. D. Lokhande, *Electrochim. Acta*, 2013, **98**, 32.
3 Q. Yang, Z. Lu, X. Sun and J. Liu, *Sci. Rep.*, 2013, **3**, 3537.
4 S. Chen, J. Zhu, X. Wu, Q. Han and X. Wang, *ACS Nano*, 2010, **4**, 2822.
5 G. Wang, L. Zhang and J. Zhang, *Chem. Soc. Rev.*, 2012, **41**, 797.
6 L. Wang, Z. H. Dong, Z. G. Wang, F. X. Zhang and J. Jin, *Adv. Funct. Mater.*, 2012, **23**, 2758.
7 C. Zhao, X. Wang, S. Wang, Y. Wang, Y. Zhao and W. Zheng, *Int. J. Hydrogen Energy*, 2012, **37**, 11846.
8 M. Zhi, C. Xiang, J. Li, M. Li and N. Wu, *Nanoscale*, 2012, **5**, 72.
9 C. Zhao, W. Zheng, X. Wang, H. Zhang, X. Cui and H. Wang, *Sci. Rep.*, 2013, **3**, 2986.
10 H.-W. Wang, Z.-A. Hu, Y.-Q. Chang, Y.-L. Chen, Z.-Y. Zhang, Y.-Y. Yang and H.-Y. Wu, *Mater. Chem. Phys.*, 2011, **130**, 672.
11 Z. Li, J. Wang, L. Niu, J. Sun, P. Gong, W. Hong, L. Ma and S. Yang, *J. Power Sources*, 2014, **245**, 224.
12 S. Chen, J. Zhu and X. Wang, *J. Phys. Chem. C*, 2010, **114**, 11829.
13 J. Jiang, J. Liu, R. Ding, J. Zhu, Y. Li, A. Hu, X. Li and X. Huang, *ACS Appl. Mater. Interfaces*, 2011, **3**, 99.
14 R. R. Salunkhe, B. P. Bastakoti, C.-T. Hsu, N. Suzuki, J. H. Kim, S. X. Dou, C.-C. Hu and Y. Yamauchi, *Chem. – Eur. J.*, 2014, **20**, 3084.
15 C. Yuan, L. Yang, L. Hou, L. Shen, X. Zhang and X. W. Lou, *Energy Environ. Sci.*, 2012, **5**, 7883.
16 Y.-L. Wang, Y.-Q. Zhao and C.-L. Xu, *J. Solid State Electrochem.*, 2011, **16**, 829.
17 Y. Zhang, X. Xia, J. Kang and J. Tu, *Chin. Sci. Bull.*, 2012, **57**, 4215.
18 S. H. Lee, J. R. Harding, D. S. Liu, J. M. D'Arcy, Y. Shao-Horn and P. T. Hammond, *Chem. Mater.*, 2014, **26**, 2579.
19 C.-C. Sung, C.-Y. Liu and C. C. J. Cheng, *Int. J. Hydrogen Energy*, 2014, **39**, 11706.
20 S. Gao, J. Zhong, G. Xue and B. Wang, *J. Membr. Sci.*, 2014, **470**, 316.
21 D. Wei, J. Liang, Y. Zhu, Z. Yuan, N. Li and Y. Qian, *Part. Part. Syst. Charact.*, 2013, **30**, 143.
22 J. R. Neilson, B. Schwenzer, R. Seshadri and D. E. Morse, *Inorg. Chem.*, 2009, **48**, 11017.
23 S.-L. Chou, J.-Z. Wang, H.-K. Liu and S. X. Dou, *J. Electrochem. Soc.*, 2008, **155**, A926.
24 L.-B. Kong, M.-C. Liu, J.-W. Lang, M. Liu, Y.-C. Luo and L. Kang, *J. Solid State Electrochem.*, 2010, **15**, 571.
25 D. Ghosh, S. Giri and C. K. Das, *ACS Sustainable Chem. Eng.*, 2013, **1**, 1135.
26 J. Fang, M. Li, Q. Li, W. Zhang, Q. Shou, F. Liu, X. Zhang and J. Cheng, *Electrochim. Acta*, 2012, **85**, 248.
27 X. Wang, C. Yan, A. Sumboja, J. Yan and P. S. Lee, *Adv. Energy Mater.*, 2013, **4**, 1301240.
28 X.-C. Dong, H. Xu, X.-W. Wang, Y.-X. Huang, M. B. Chan-Park, H. Zhang, L.-H. Wang, W. Huang and P. Chen, *ACS Nano*, 2012, **6**, 3206.
29 C.-Y. Sun, Y. G. Zhu, T.-J. Zhu, J. Xie, G.-S. Cao and X.-B. Zhao, *J. Solid State Electrochem.*, 2013, **17**, 1159.

30 X. Lu, D. Zheng, T. Zhai, Z. Liu, Y. Huang, S. Xie and Y. Tong, *Energy Environ. Sci.*, 2011, **4**, 2915.
31 Z. Liu, R. Ma, M. Osada and K. Takada, *J. Am. Chem. Soc.*, 2005, **127**, 13865.
32 C. Nethravathi, C. R. Rajamathi, M. Rajamathi, X. Wang, U. K. Gautam, D. Golberg and Y. Bando, *ACS Nano*, 2014, **8**, 2755.
33 L.-X. Yang, Y.-J. Zhu, L. Li, L. Zhang, H. Tong, W.-W. Wang, G.-F. Cheng and J.-F. Zhu, *Eur. J. Inorg. Chem.*, 2006, **2006**, 4787.
34 Z. Chen, Y. Chen, C. Zuo, S. Zhou, A. G. Xiao and A. X. Pan, *Bull. Mater. Sci.*, 2013, **36**, 239.
35 D. Guo, E. Shangguan, J. Li, T. Zhao, Z. Chang, Q. Li, X.-Z. Yuan and H. Wang, *Int. J. Hydrogen Energy*, 2014, **39**, 3895.
36 C.-W. Tang, C.-B. Wang and S.-H. Chien, *Thermochim. Acta*, 2008, **473**, 68.
37 J. Yang, H. Liu, W. N. Martens and R. L. Frost, *J. Phys. Chem. C*, 2010, **114**, 111.
38 X. Wang, S. Liu, H. Wang, F. Tu, D. Fang and Y. Li, *J. Solid State Electrochem.*, 2012, **16**, 3593.
39 W. S. Hummers Jr. and R. E. Offeman, *J. Am. Chem. Soc.*, 1958, **80**, 1339.
40 H. Wang, Q. Hao, X. Yang, L. Lu and X. Wang, *Electrochem. Commun.*, 2009, **11**, 1158.